Characterization and Application of Magnetic Biochars from Corn Stalk by Pyrolysis and Hydrothermal Treatment

Yuting Tu, Zhiping Peng, Peizhi Xu, Huanjia Lin, Xuena Wu, Linxiang Yang, and Jichuan Huang *

Two novel magnetic biochar composites (FeC-H and FeC-P) were synthesized using corn stalks and ferrous sulfate through hydrothermal method and traditional pyrolysis, respectively. The samples were characterized by Fourier transform infrared spectroscopy (FTIR), X-ray powder diffraction (XRD), vibrating sample magnetometer, and particle size analyzer. Batch experiments were conducted to investigate the ability of those samples to absorb aqueous phosphate. FeC-H had lower surface area than FeC-P, but more hydrophilic functional groups were detected on the rough surface of FeC-H. The impregnated iron was present as Fe_3O_4 in the prepared magnetic biochar composites. The introduced Fe_3O_4 resulted in high performance of magnetic separation and also played the role as adsorption sites for phosphate. FeC-H and FeC-P demonstrated higher sorption capacity than bare Fe_3O_4 due to the highly dispersed and smaller crystalline sizes of Fe_3O_4 particles loaded in corn stalk derived-biochar support. FeC-H had the best performance, with Langmuir adsorption capacity as high as 5.04 mg/g for phosphate. These results indicate that the magnetic biochar composites prepared from corn stalks by hydrothermal method (FeC-H) have potential as a high-efficiency and cost-effective adsorbent for phosphorus removal from wastewater.

INTRODUCTION

Corn is one of the main food crops in China, and about 250 million tons of corn stalks is produced annually. Currently, most of these agricultural residues are discarded as waste or by incineration (Xing *et al.* 2016). Compared with the traditional methods, converting the corn stalks into biochars is a more promising solid biomass waste disposal strategy, considering its large yield, high carbon content, and low ash content. A number of studies have demonstrated the feasibility of using those biomass wastes as raw materials for the preparation of biochar. High-temperature pyrolysis and hydrothermal treatment are the most commonly applied methods for the conversion of biomass into carbonized materials. Pyrolysis is usually carried out by using dry feedstock at temperatures between 500 to 950 °C under O_2-free conditions. In low-temperature hydrothermal carbonization, the biomass is mixed with water and treated at temperatures in the range 170 to 300 °C

under pressure. Compared with conventional pyrolysis, less energy is needed in hydrothermal carbonization because prior drying of the feedstocks is not required, and the treatment temperature is much lower (Peterson *et al.* 2008). The biochars prepared by these two thermal processes have been extensively investigated for use as adsorbents for the removal of toxic metal ions in aqueous solutions, such as Cr, Cu, Pb, Cd, Hg, Fe, and Zn, and non-biodegradable organic pollutants including dyes, phenollics, pesticides, polynucelar aromatics, and antibiotics (Libra *et al.* 2011; Mohan *et al.* 2014).

There are differences between the two types of biochars. Liu *et al.* (2010) used the hydrothermal char (H300) and pyrolytic char (P700) produced from pinewood as adsorbents for the copper in water. Comparative experiments revealed that the predominant copper adsorption mechanism for H300 was ion-exchange reaction, while P700 mainly used physical surface adsorption. Sun *et al.* (2011) prepared thermal and hydrothermal biochars from poultry and animal manures. They found that the hydrothermal biochars presented higher sorption capacity of bisphenol A (BPA), 17α-ethinyl estradiol (EE2), and phenanthrene (Phen) than thermally produced biochars due to the existence of diverse functional groups and more amorphous aliphatic-carbon. Fuertes *et al.* (2010) observed similar results after comparing the main properties of biochar obtained after pyrolysis and hydrochar of corn stover. The study revealed that atomic O/C and H/C ratios in the hydrochar were higher than that in the biochar, and higher aromatic carbon and ash content were detected in biochar.

However, powdered biochar is difficult to separate from the aqueous solution in practical applications. A promising strategy for resolving this problem is introducing magnetic medium (*e.g.*, magnetite, γ-Fe_2O_3, and α-FeOOH) to the carbon phase. The prepared magnetic biochar composites can be effectively separated and recovered upon the application of a magnetic field. Hence, the synthesis and application of magnetic biochar composites have attracted intense attention. The most widely studied synthesis approach is pyrolysis. Recently, several studies have reported the preparation of magnetic carbon composites by hydrothermal conversion, but most of them used glucose as a carbon source (Zhu and Diao 2011; Jazirehpour and Ebrahimi 2015). There is little research focused on the application of waste biomass as carbon source for the preparation of magnetic biochars. Using waste biomass to synthesis magnetic biochar materials through hydrothermal processes could be an energy-saving and environmentally friendly method.

The processes of carbonization and magnetization during pyrolysis and hydrothermal treatment for the preparation of magnetic biochar samples take place under very different conditions. Differences in characteristics of the solid obtained materials are to be expected. In this study, corn stalk was selected as a representative of waste biomass. Two types of magnetic chars were synthesized by pyrolysis and hydrothermal method for comparison. Fourier transform infrared spectroscopy (FTIR), X-ray powder diffraction (XRD), vibrating sample magnetometry, and particle size analysis were employed to characterize the samples. Excess phosphate is a typical contaminant in wastewater that can result in significant eutrophication. The combined magnetic iron oxide has potential to enhance the sorption ability of phosphate (Chen *et al.* 2011). Hence, the prepared magnetic biochar composites were applied as adsorbents for phosphate removal from aqueous solution, and the difference in adsorption abilities was investigated. The objectives of this study were to determine the different characteristics of magnetic biochars from corn stalk by pyrolysis and hydrothermal treatment, and further evaluate its potential to be utilized for removal of aqueous phosphorus.

EXPERIMENTAL

Materials

Analytical grade ferrous sulfate ($FeSO_4 \cdot 7H_2O$), sodium thiosulfate ($Na_2S_2O_3$), potassium phosphate monobasic (KH_2PO_4), H_2SO_4, and NaOH were obtained from Guangzhou Chemical Reagent Company, Guangzhou, China. Corn stalks were obtained from Zhongluotan base farm in the Conghua District of Guangzhou, China. The corn stalks were dried at 105 °C to a constant weight, ground, sifted through an 80-mesh sieve, and stored in a desiccator. Chemical analysis of the corn stalk showed that it contained 5.7 wt.% ash, 35.7 wt.% cellulose, 30.3 wt.% hemicelluloses, and 11.5 wt.% lignin.

Preparation of the Magnetic Carbon Composites

Two different methods were used to prepare the corn stalks derived biochar using supported iron oxide composites. In the first method, magnetic biochar composites were prepared by hydrothermal treatment (named FeC-H). A total of 4.0 g of corn stalk powder, 6.0 mmol $FeSO_4$, and 6.0 mmol of $Na_2S_2O_3$ was dissolved in 20 mL of distilled water. The mixture was vigorously stirred, and 45 mL of 0.3 mol/L NaOH solution was added dropwise at the same time. The precursor solution was transferred into a Teflon-lined stainless steel autoclave, which was heated at 220 °C for 3 h. After cooling the autoclave to room temperature, the deposit was separated by centrifugation, washed with distilled water and ethanol several times, and dried at 60 °C for 4 h in vacuum.

The catalyst was also synthesized *via* pyrolysis (named as FeC-P). The precursor solution was prepared in the same way as in the hydrothermal method and then dried overnight at 60 °C in vacuum. Subsequently, the received solid was pyrolyzed under flowing nitrogen in a horizontal furnace at 650 °C for 3 h (heating rate: 20 °C/min). The pyrolyzed sample was also washed and dried.

For comparison, the companion biochars without iron oxide were also prepared by the same hydrothermal or pyrolysis process. The obtained biochar samples are referred to as C-H and C-P, respectively. All four kinds of samples were passed through a 200-mesh sieve and stored in a desiccator prior to use.

Characterization of the Samples

The ash contents of samples were determined using a standard method according to ASTM D2866-94. Elemental analyses of C and H for the prepared samples were carried out using an Elementar Vario EL Cube analyser (Elementar Analysensysteme GmbH, Langenselbold, Germany). The pH of the point of zero charge (pH_{PZC}) of the prepared samples were determined by adding increasing amounts of solid sequentially into a 50 mL 0.0005 M NaCl solution until the pH reached a plateau (Tu *et al.* 2014). The CEC values were measures by the standard exchange method with ammonium acetate (Chamuah and Dey1982). The iron content of the synthesized samples was measured by a flame atomic absorption spectrophotometer (model ZA3300, Hitachi, Tokyo, Japan). The surface area was determined through a multipoint Brunauer-Emmett-Teller (BET) method using a surface area analyzer (Autosorb-1, Quantachrome, Boynton Beach, FL, USA). Fourier transform infrared (FTIR) spectroscopy was recorded on a Bruker EQUINOX55 FTIR spectrophotometer (Bruker GmbH, Karlsruhe, Germany) from 4000 to 400 cm^{-1}. The chemical state of iron on the samples was determined by X-ray diffraction (XRD) using a D/Max 2200 VPC diffraction meter (D/Max 2200 VPC, Rigaku, Tokyo, Japan) with Cu

Kα radiation. Information about the types of oxygen-containing functional groups on the surface of the prepared magnetic biochars was obtained by an X-ray photoelectron spectroscopy (Thermo K-Alpha XPS, Thermo Fisher Scientific, West Palm Beach, FL, USA). The morphology of the samples was determined by phase-contrast microscopy (Zeiss) and by scanning electron microscopy (SEM) (PhilipsXL-30 ESEM FEG, Philips, Eindhoven, Netherlands). The magnetic measurement was carried out with a vibrating sample magnetometer (VSM) (BHV-55, Riken, Japan). The average particle size was obtained by a particle size analyzer (Mastersizer-2000, Malvern Instruments Ltd., Malvern, UK).

Phosphorus Adsorption and Desorption Experiments

Adsorption isotherms of prepared samples to aqueous phosphate were determined through batch sorption experiments. Phosphate solution with various initial concentration of P ranged from 5 to 40 mg/L were prepared by dissolving KH_2PO_4 in deionized water. Next, 0.125 g of each adsorbent and 50 mL phosphate solution were added into 250-mL stoppered flasks. The flasks were shaken at 180 rpm in the dark under 25 °C for 24 h for all adsorbents to achieve equilibrium, and the suspensions were centrifuged and further filtered through a 0.22 µm Millipore membrane filter. The phosphate concentration in the solution was determined by ammonium molybdate spectrophotometric method at 700 nm on a Metash V-5000 spectrophotometer (Shanghai, China). All experiments were performed in duplicate, and the average values with a relative standard deviation of less than 5% were presented.

The test of phosphate desorption were conducted with initial phosphate concentrations of 5, 20, and 40 mg P/L. After the adsorption experiments, the remaining exhausted adsorbent was air dried and 50 mL 0.01 mol/L KCl was added as external solution for the phosphate desorption studies. The mixtures were shaken for 24 h at 25 °C. Then the suspension solution was centrifuged and the concentration of desorbed phosphate was analyzed. The procedure was repeated until P concentration in the supernatant liquid reached undetectable levels (< 0.01 mg/L) and the total amount of desorbed phosphate was calculated.

RESULTS AND DISCUSSION

Characterization of the Magnetic Carbon Composites

The basic physical and chemical characteristics of the FeC-H, FeC-P, C-H, and C-P are summarized in Table 1. Compared with C-P and FeC-P, C-H and FeC-H had higher yield, lower ash content, and higher H/C ratio. This result reflected that more original organic matter was preserved in the samples prepared by hydrothermal treatment in comparison with the pyrolyzed materials, and pyrolysis allowed deeper carbonization than hydrothermal treatment (Liu *et al.* 2010). Thus, the iron content in FeC-P was higher than in FeC-H. And more basic surface property (higher pH_{PZC} values) was observed for the samples obtained after high temperature pyrolysis. Furthermore, the samples obtained after pyrolysis exhibited higher specific surface area than the hydrothermal treatment samples. The BET specific surface area for FeC-P was about twice that of C-P. This could be attributed to the pore production effect of sulfates on the biochar support during pyrolysis treatment. The impregnated sulfates produce SO_3 during the thermal treatment, which

decomposes to SO_2 and O_2. The produced O_2 reacted with the biochar support, hence pores in the carbon matrix were formed (Tu *et al.* 2013).

Table 1. Physicochemical Properties of the Prepared Samples

Sample	Yield [a] (wt.%)	Ash Content (wt.%)	C (wt.%)	H (wt.%)	H/C	pH_{PZC}	CEC (cmol/kg)	Fe (wt.%)	S_{BET} (m^2/g)
C-H	37.2	3.4	58.28	5.81	0.099	5.05	11.95	-	18.9
FeC-H	63.2	19.6	30.80	3.09	0.100	5.58	11.10	12.8	16.6
C-P	24.5	16.8	70.86	1.52	0.021	8.96	7.42	-	158.0
FeC-P	46.5	33.3	24.69	1.63	0.062	7.64	6.44	17.4	303.1
[a] Yield expressed as (g product/100 g corn stalk feedstock)									

Figure 1a shows the FTIR spectra of corn stalk and the prepared materials. In the spectrum for C-H and FeC-H, overlapping bands at 1430 to 1420 cm^{-1}, 1375 cm^{-1}, and 1250 cm^{-1} were assigned to the finger print regions of lignin (–O–CH$_3$ deformation vibration), cellulose (–CH deformation vibration), and hemicellulose (C–O stretching vibration) (Zhang *et al.* 2015; Khandanlou *et al.* 2016). Compared with raw corn stalk precursor, the diminishing intensity of those characteristic bands implied that some part of hemicellulose, cellulose, and lignin in C-H and FeC-H were degraded during hydrothermal treatment. The peaks at 3400 cm^{-1} (–OH stretching vibrations), 2926 cm^{-1} (–CH$_3$ stretching vibration), 2864 cm^{-1} (–CH$_2$ stretching vibration), 1640 cm^{-1} (C=O stretching vibration), and 1040 cm^{-1} (–OH bending vibrations) (Sevilla and Fuertes 2009) became sharp and intense, indicating that a large number of polar groups remained on the surface of hydrothermal treated samples. These hydrophilic functional groups denoted significant hydrophilic character of C-H and FeC-H. For the FTIR curves of C-P and FeC-P, all the peak intensities were diminished after treatment, showing that the surface feature of C-P and FeC-P were reconstructed during high-temperature pyrolysis. Liu *et al.* (2010) observed similar FTIR results in biochars produced from pinewood by pyrolysis and hydrothermal treatment. The total amount of oxygen-containing groups on the surface of pinewood-derived solid sample increased 95% after hydrothermal treatment, while 56% of oxygen-containing groups decreased after pyrolysis. In addition, a new peak appeared at 580 cm^{-1} in the FTIR curves of both FeC-H and FeC-P compared with corresponding biochars. This peak is a characteristic signal of the stretching vibration of Fe–O (Wang *et al.* 2014), indicating the introduction of iron oxides into the composites.

To further confirm the iron chemical state in the magnetic biochar composites, XRD analysis was conducted for FeC-P, FeC-H, and the Fe_3O_4 prepared by hydrothermal method (Fe_3O_4-H), as presented in Fig. 1b. In all three XRD patterns, the peaks at 2θ of 30.1°, 35.4°, 43.1°, 56.9°, and 62.5° matched well with the standard peak values of magnetite (JCPDS Card no.19-0629) (Zhang *et al.* 2008), indicating that the iron oxide particles were identified as magnetite. There were obvious differences in peak intensity and width between these three samples. The intensity of the XRD peaks decreased and the width increased when Fe_3O_4 particles were modified with corn stock derived biochar, indicating that the average crystalline sizes of magnetic Fe_3O_4 particles were changed. The broadness of the XRD peaks was used to calculate the average crystalline size of Fe_3O_4 particles using the Debye-Scherrer formula. The crystalline sizes of FeC-H and FeC-P were 9.7 and 25.1 nm, smaller than that of the bare Fe_3O_4 particles (33.2 nm).
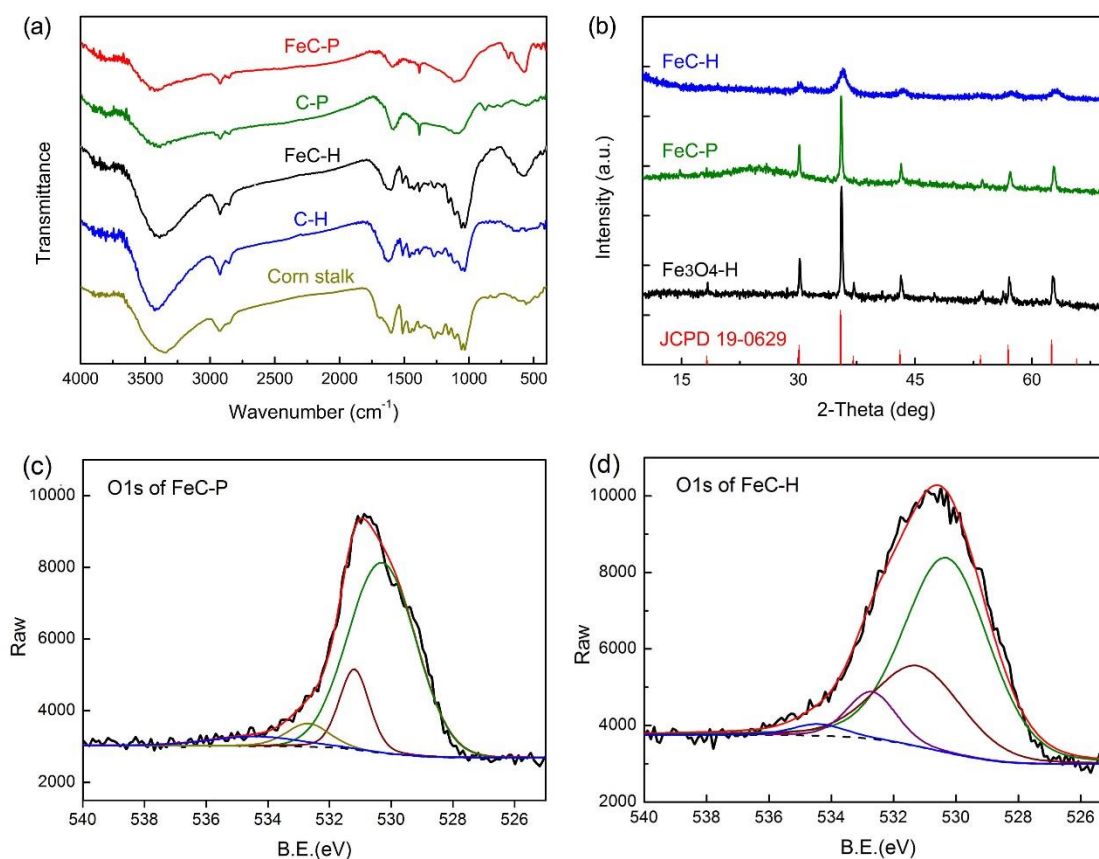
Fig. 1. (a) FTIR spectra of corn stalk, magnetic biochars, and the corresponding biochars prepared by pyrolysis and hydrothermal treatment. (b) XRD patterns of FeC-H, FeC-P and Fe$_3$O$_4$-H. XPS patterns of the O1s region and deconvolution of the corresponding peaks for FeC-P (c) and FeC-H (d).

Table 2. Results of Deconvolution of the O1s Band in the XPS Spectra

Sample		530.3 eV (Lattice oxygen (O^{2-}) in Fe$_3$O$_4$)	531.2 eV (-OH)	532.5 eV (CO$_3^{2-}$)	532.7 eV (C=O)	534.4 eV (COOH)
FeC-P	Peak area (CPS.eV)	14883.9	3784.0	1348.0		644.3
	Relative content (at.%)	72.0	18.3	6.5		3.1
FeC-H	Peak area (CPS.eV)	19087.5	8093.1	-	2631.9	696.9
	Relative content (at.%)	62.6	26.5	-	8.6	2.3

The XPS spectrum of the O1s region for FeC-P and FeC-H are shown in Fig. 1c and 1d, and the results of multiple region peak fitting of the O1s band are given in Table 2. The O1s peak was deconvoluted into four peaks. The peak located at lower binding energy (530.3 eV) can be attributed to the lattice oxygen (O^{2-}) in the Fe$_3$O$_4$ (Bouanis *et al.* 2009). As shown in Table 2, the peak area of crystal lattice oxygen for FeC-H was 1.28 times larger than that of FeC-P, indicating that there was a higher amount of Fe$_3$O$_4$ particles on the surface of FeC-H than FeC-P. The other three peaks located at 531.2–534.4 eV could

be attributed to surface oxygen containing functional groups. The amount of hydroxyl groups (-OH) and carboxyl acid groups (COOH) on the surface of FeC-H were 2.14 and 1.08 times as large as that of FeC-P calculated by peak area, which is consistent with the results of FTIR. Under the best optimization of multiple region peak fitting, peaks located at 532.7 eV assigned to carboxyl groups (C=O) was detected on FeC-H, while 532.5 eV attributed to carbonate was observed on FeC-P. The high amount of acidic oxygen containing groups on the surface of FeC-H and basic carbonate on FeC-P would be the cause of the different pH_{PZC} values for FeC-H and FeC-P (5.58 and 7.64).

The SEM micrographs of raw corn stock powder, bare Fe_3O_4-H, FeC-P, and FeC-H are shown in Fig. 2. Compared with the raw corn stock (Fig. 2a), the particle size of FeC-P and FeC-H was much smaller (Fig. 2c and 2e). Furthermore, the enlarged SEM micrograph of FeC-P (Fig. 2d) clearly reveals that pores were present on the surface of the sample. FeC-H had the relatively rough exterior surface morphology covered with micron-sized spherical Fe_3O_4 particles (Fig. 2f). This variation showed that the morphological features were strongly influenced by the preparation methods. For FeC-P, pores were produced from the thermal decomposition of biomass and sulfates after high temperature pyrolysis. This result was consistent with the different S_{BET} values of FeC-P and FeC-H. For FeC-H, FTIR analysis confirmed that the carbon phase formed from hydrothermal synthesis was rich in oxygenated functional groups on the exterior surface, and those functional groups provide thermodynamically favorable nucleation sites for the nucleation and growth of Fe_3O_4 nanoparticles during the hydrothermal process (Zubir *et al.* 2014). Hence, more Fe_3O_4 particles were adhered to the surface of FeC-H.

As shown in Fig. 2b, the bare Fe_3O_4 nanoparticles, with an average size of 34 nm, were aggregated into spherical particles with the size of 0.98 μm. After the addition of biochar support, no severe Fe_3O_4 aggregation was observed for FeC-P and FeC-H. To further confirm the distribution of loaded Fe on the surface of magnetic biochars, EDX mapping were carried out, and the results are presented in Fig. 2g and 2h. It was found that the distribution of Fe on the surface of FeC-H was more intensive and uniform than FeC-P. This phenomenon was in good agreement with the results obtained by XRD analysis. Therefore, the biochar support could provide a matrix for dispersion of Fe_3O_4 nanoparticles and prevent the aggregation of those small particles.

The typical magnetic hysteresis loops measured at room temperature are depicted in Fig. 3a. The samples presented a magnetization saturation value (Ms) of 11.2, 20.4, and 63.9 emu/g for FeC-H, FeC-P, and bare Fe_3O_4-H, respectively. The Ms values of magnetic biochar composites were much smaller than that of bare Fe_3O_4. This is because the biochar support reduced the proportion of Fe_3O_4 in the prepared composite samples, hence decreasing the magnetization (Jazirehpour and Ebrahimi 2015). In contrast, the smaller particle size in the magnetic biochar composites compared with bare Fe_3O_4 particles is another cause of lower Ms value (Wang *et al.* 2011). Even though the use of carbon support affected the total magnetization of the magnetic composite samples, they still allowed easy separation from the reaction medium by a magnet (inset of Fig. 3a). Furthermore, the particle size distribution of Fe_3O_4-H, FeC-P, and FeC-H were measured (Fig. 3b). The average particle size of Fe_3O_4-H, FeC-P, and FeC-H were 1483, 779, and 233 nm, respectively. Compared with the micron-sized Fe_3O_4 particles shown in the SEM images (Fig. 2b), the bulk Fe_3O_4 particles were prone to further aggregation, forming larger particles when dispersed in the deionized water. Better dispersion of FeC-H in water could be attributed to the strong surface hydrophilicity and its lower magnetization.
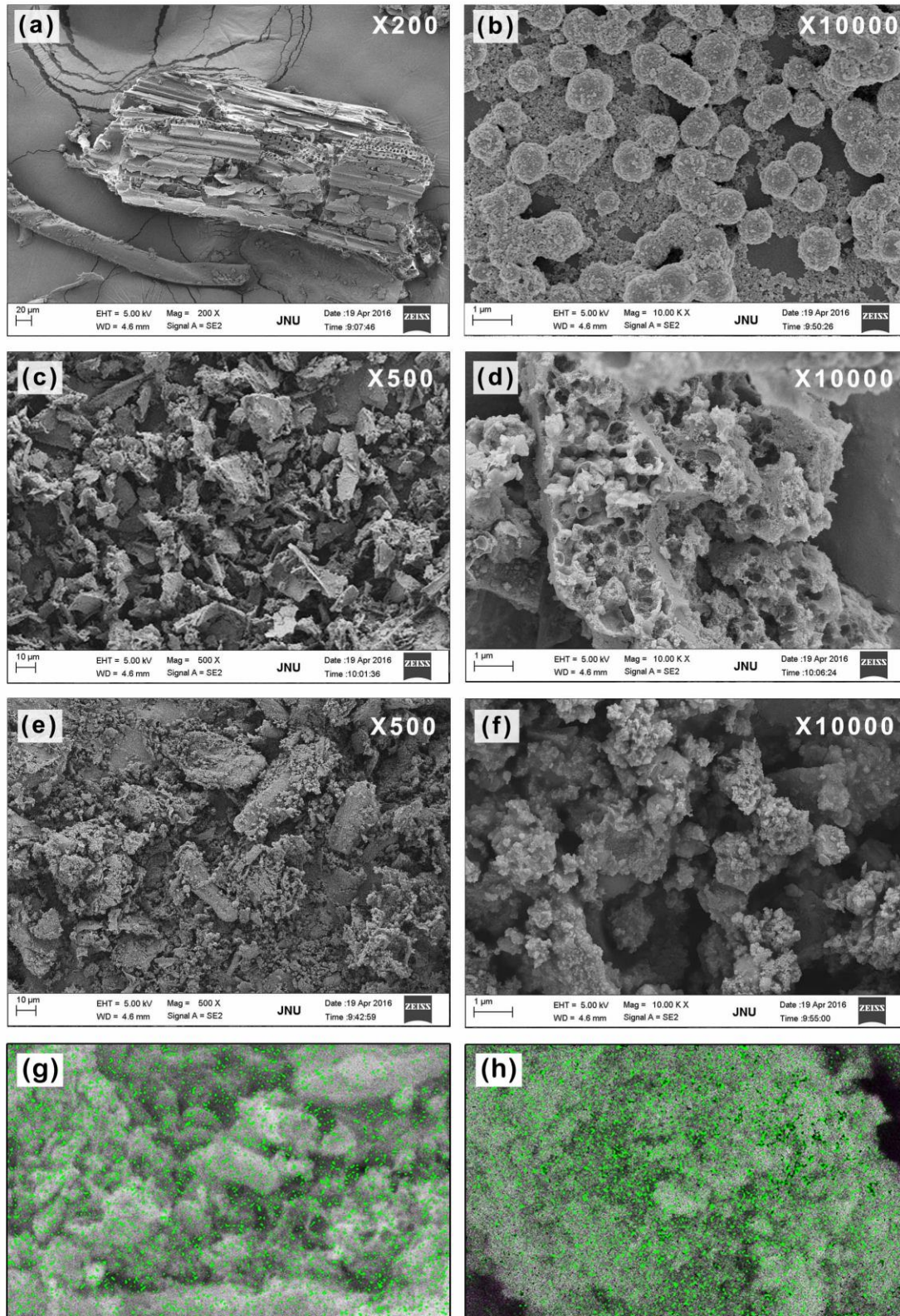
Fig. 2. SEM micrographs of (a) corn stalk feedstock, (b) Fe_3O_4 prepared by hydrothermal method, (c) and (d) magnetic biochar produced from pyrolysis, (e) and (f) magnetic biochar produced from hydrothermal treatment, (g) and (h) Fe mapping of FeC-P and FeC-H by EDX analysis
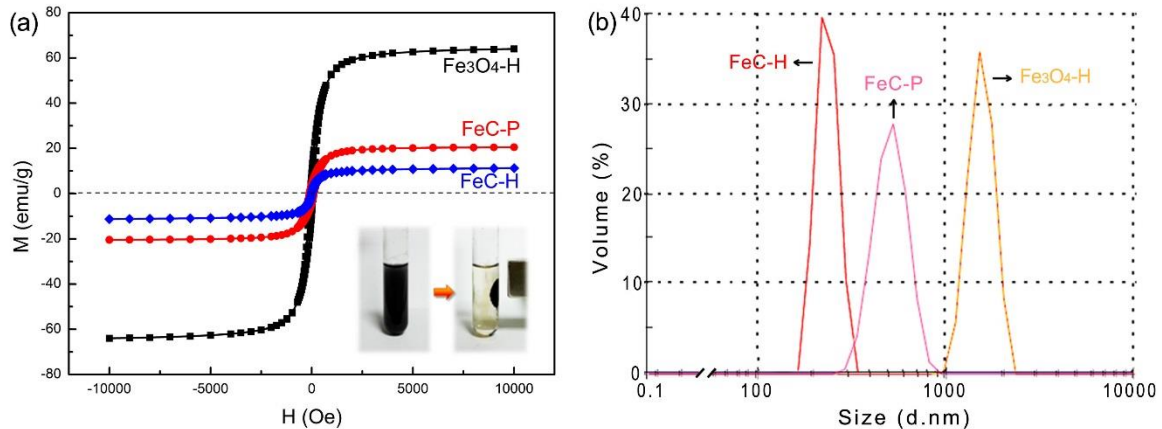
Fig. 3. (a) Magnetic hysteresis loop of Fe₃O₄-H, FeC-P, and FeC-H. The inset shows the magnetic separation of FeC-H; (b) Particle size distributions of Fe₃O₄-H, FeC-P, and FeC-H

Phosphate Adsorption and Desorption

The phosphate sorption isotherms of C-H, C-P, Fe₃O₄-H, FeC-H, and FeC-P are presented in Fig. 4a. C-H and C-P showed a relatively low capacity for phosphate removal. For FeC-H and FeC-P, the adsorption capacity was greatly enhanced when Fe₃O₄ was introduced into biochar supports. This result indicated that the sorption of the phosphate was dominated by the iron oxides rather than biochar components. To further elucidate the sorption behavior of magnetic biochar composites, the sorption data of Fe₃O₄-H, FeC-H and FeC-P was further fitted by Langmuir and Freundlich models. The isotherms of Langmuir and Freundlich models are represented by Eqs. 1 and 2,

$$q_e = \frac{Q_0 C_e}{1/b + C_e}$$

(1)

$$q_e = K_f C_e^{1/n}$$

(2)

where q_e is the amount of phosphate adsorbed at equilibrium (mg/g), C_e is the equilibrium concentration (mg/L), and Q_0 and b are Langmuir constants, which are indicators of the maximum adsorption amounts and energy of adsorption, respectively. K_f and n are the Freundlich constants related to adsorption capacity and adsorption intensity, respectively.
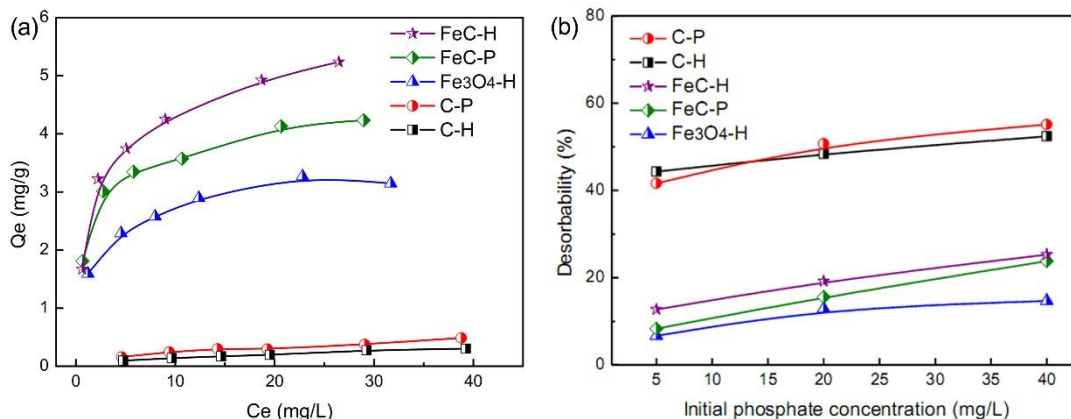

Fig. 4. (a) Adsorption isotherms of prepared samples; (b) Desorbability of the adsorbed phosphate on different adsorbents

The adsorption coefficients are listed in Table 3. The adsorption of phosphate on all the adsorbents fitted better to the Langmuir model rather than the Freundlich model. The maximum adsorption capacity calculated from Langmuir model was 5.04 mg/g for FeC-H, 4.07 mg/g for FeC-P, and 3.15 mg/L for Fe_3O_4-H. FeC-H presented the best phosphate sorption capacity. Even though biochar did not show obvious adsorption of phosphate, employing biochar as support could prevent the aggregation of Fe_3O_4 and provide more accessible adsorption sites for phosphate. Hence, FeC-H and FeC-P presented higher phosphate adsorption capacity than bare Fe_3O_4-H. Furthermore, a difference in sorption was observed between FeC-H and FeC-P.

Table 3. Nonlinear Langmuir and Freundlich Adsorption Constants of Phosphate on Three Magnetic Materials

Adsorbent	Langmuir Parameters			Freundlich Parameters		
	Q_0 (mg/g)	b (L/mg)	r^2	K_f (mg/g)	n	r^2
Fe_3O_4-H	3.16	0.82	0.9731	1.62	4.62	0.9485
FeC-P	4.07	1.21	0.9837	2.18	4.63	0.9436
FeC-H	5.04	0.80	0.9929	2.20	3.47	0.9368

In order to reveal the adsorption mechanism of phosphate, the phosphate adsorption capacity of commercial activated carbon has also been examined for comparison. The maximum phosphate adsorption capacity was calculated to be 0.41 mg/g. Hence, adsorption of phosphate mainly on iron oxides is likely the key mechanism for phosphate removal using the magnetic biochars.

Other studies found that the sorption mechanism of phosphate on magnetite is through electrostatic interaction or ligand exchange of the phosphate anions with hydroxide iron oxide surfaces (Antelo *et al.* 2005). The different adsorption capacities of FeC-H and FeC-P for phosphate were probably related with their different physicochemical properties. Firstly, the phosphate adsorption capacity of the magnetite composite has been found to be strongly related with the surface amount of iron (Daou *et al.* 2007). As evidenced by XRD, XPS and SEM analysis, more numbers and smaller size of Fe_3O_4 nanoparticles with large surface energy were uniformly distributed in FeC-H than in FeC-P, indicating that FeC-H would have much more phosphate binding sites on the surface than FeC-P. On the other hand, the different surface acidity and pH_{PZC} values would another reason for the different phosphate adsorption capacity between FeC-H and FeC-P. The pH_{PZC} of Fe_3O_4 is 6.2 (Fu *et al.* 2015), which indicates that the surface of Fe_3O_4 nanoparticles was positively charged when solution pH was lower than pH_{PZC}, and negatively charged when solution pH above pH_{PZC}. In our experiments, pH values of the solutions with different initial phosphate concentration after adsorption was measured, the pH for FeC-H containing suspensions were 4.6-5.2, and 6.3-7.2 for FeC-P containing suspensions. This variation in solution pH was probably related with the different pH_{PZC}. When using FeC-H as adsorbents, the Fe_3O_4 nanoparticles in FeC-H carry positive charges. The dominant form of phosphorous is $H_2PO_4^-$ in FeC-H containing suspensions. Hence, the adsorption of negatively charged phosphate ions by positive charged Fe_3O_4 nanoparticles is favorable due to the electrostatic attraction. While, the Fe_3O_4 nanoparticles are more negatively in FeC-P containing solutions. Furthermore, some of the phosphorous changes into more negatively charged HPO_4^{2-} when solution pH higher than 6.0. The electrostatic repulsion between the

negatively charged surface of Fe_3O_4 nanoparticles in FeC-P and the HPO_4^{2-} would result in the lower P adsorption capacity than FeC-H.

The desorbability of P can be defined as the percent of the desorbed P over the total adsorbed P by the adsorbent. The desorbability is shown in Fig. 4b. For all the adsorbents, the amount of the desorbed P is slightly increased with the increase of the initial concentration of P. Around 40 to 55% of phosphate desorbed from C-P and C-H, while the desorbability of P for Fe_3O_4-H, FeC-P, and FeC-H was lower than 24%. The low desorbability capacity of iron oxides were also confirmed by Daou *et al.* (2007). These results indicated that the P adsorption on the Fe_3O_4 containing materials was stronger than pure carbon adsorbents. Furthermore, the low desorbability of FeC-P and FeC-H also demonstrated that phosphate was mainly adsorbed by Fe_3O_4 partials in the magnetic biochar composites.

The experimental results gave evidence that the synthesized FeC-H exhibited effective phosphate adsorption capacity and high magnetic separation ability. Furthermore, the FeC-H was derived from agricultural biomass wastes and synthesized by energy saving hydrothermal method. Thus, it can be considered as an economically feasible and eco-friendly magnetic biochar adsorbent. It also shows the potential application for the removal of excess aqueous phosphate generated from industrial, agricultural, or household sources to control the eutrophication of surface water.

CONCLUSIONS

1. The magnetic biochars were synthesized *via* hydrothermal and pyrolysis processes in one step through simultaneous carbonization and magnetization. The magnetic biochar composite prepared by the hydrothermal method (FeC-H) contained many more oxygen-containing groups on the surface than the samples treated after pyrolysis.

2. Compared with bare Fe_3O_4, there were higher distribution and smaller crystalline sizes of Fe_3O_4 in the magnetic biochar composites FeC-H and FeC-P due to the biochar support.

3. In this study, sorption capabilities of phosphate were in the sequence of FeC-H > FeC-P > Fe_3O_4-H > C-P > C-H. FeC-H exhibited the highest adsorption capacity despite the fact that it had lower surface area compared with FeC-P. The highest adsorption capacity of FeC-H was 5.04 mg/g.

4. Due to its high phosphate adsorption capacity and low cost, the magnetic biochar composites prepared from corn stalks by hydrothermal method (FeC-H) has the potential to be utilized for removal of phosphorus from wastewater.

ACKNOWLEDGMENTS

REFERENCES CITED

ASTM D570-98 (2010). "Standard test method for water absorption of plastics," ASTM International, West Conshohocken, USA.

Antelo, J., Avena, M., Fiol, S., Lopez, R., and Arce, F. (2005). "Effects of pH and ionic strength on the adsorption of phosphate and arsenate at the goethite-water interface," *J. Colloid Interface Sci*. 285(2), 476-486. DOI: 10.1016/j.jcis.2004.12.032

Bouanis, F., Bentiss, F., Traisnel, M., and Jama, C. (2009). "Enhanced corrosion resistance properties of radiofrequency cold plasma nitrided carbon steel: gravimetric and electrochemical results," *Electrochim. Acta* 54(8), 2371-2378. DOI: 10.1016/j.electacta.2008.10.068

Chamuah, G. S., and Dey, S. K. (1982). "Determination of cation exchange capacity of woody plant roots using ammonium acetate extractant," *Plant and Soil* 68(1), 135-138. DOI: 10.1007/BF02374734

Chen, B., Chen, Z., and Lv, S. (2011). "A novel magnetic biochar efficiently sorbs organic pollutants and phosphate," *Bioresource Technol.* 102(2), 716-723. DOI: 10.1016/j.biortech.2010.08.067

Daou, T. J., Begin-Colin, S., Grenèche, J. M., Thomas, F., Derory, A., Bernhardt, P., Legaré, P., and Pourroy, G. (2007). "Phosphate adsorption properties of magnetite-based nanoparticles," *Chem. Mater.* 19(18), 4494-4505. DOI: 10.1021/cm071046v

Fu, Q., Zhou, X., Xu, L., and Hu, B. (2015). "Fulvic acid decorated Fe_3O_4 magnetic nanocomposites for the highly efficient sequestration of Ni(II) from an aqueous solution," *J. Mol. Liq*. 208(0), 92-98. DOI: 10.1016/j.molliq.2015.04.017

Fuertes, A. B., Arbestain, M. C., Sevilla, M., Maciá-Agullo, J. A., Fiol, S., López, R., Smemik, R. J., Aitkenhead, W. P., Arce, F., and Macias, F. (2010). "Chemical and structural properties of carbonaceous products obtained by pyrolysis and hydrothermal carbonisation of corn stover," *Soil Res.* 48(7), 618-626. DOI: 10.1071/SR10010

Jazirehpour, M., and Ebrahimi, S. A. S. (2015). "Carbothermally synthesized core–shell carbon–magnetite porous nanorods for high-performance electromagnetic wave absorption and the effect of the heterointerface," *J. Alloy. Compd.* 639(0), 280-288. DOI: 10.1016/j.jallcom.2015.03.160

Khandanlou, R., Ngoh, G. C., and Chong, W. T. (2016). "Feasibility study and structural analysis of cellulose isolated from rice husk: Microwave irradiation, optimization, and treatment process scheme," *BioResources* 11(3), 5751-5766. DOI: 10.15376/biores.11.2.5751-5766

Libra, J. A., Ro, K. S., Kammann, C., Funke, A., Berge, N. D., Neubauer, Y., Titirici, M. M., Fühner, C., Bens, O., Kern, J., and Emmerich, K. H. (2011). "Hydrothermal carbonization of biomass residuals: A comparative review of the chemistry, processes and applications of wet and dry pyrolysis," *Biofuels* 2(1), 89-124. DOI: 10.4155/bfs.10.81

Liu, Z., Zhang, F. S., and Wu, J. (2010). "Characterization and application of chars produced from pinewood pyrolysis and hydrothermal treatment," *Fuel* 89(2), 510-514. DOI: 10.1016/j.fuel.2009.08.042

Mohan, D., Sarswat, A., Ok, Y. S., and Pittman, C. U. (2014). "Organic and inorganic contaminants removal from water with biochar, a renewable, low cost and sustainable

adsorbent - A critical review," *Bioresource Technol.* 160(5), 191-202. DOI: 10.1016/j.biortech.2014.01.120

Peterson, A. A., Vogel, F., Lachance, R. P., Froling, M., Antal, M. J., and Tester, J. W. (2008). "Thermochemical biofuel production in hydrothermal media: A review of sub and supercritical water technologies," *Energy Environ. Sci.* 1(1), 32-65. DOI: 10.1039/B810100K

Sevilla, M., and Fuertes, A. B. (2009). "The production of carbon materials by hydrothermal carbonization of cellulose," *Carbon* 47(9), 2281-2289. DOI: 10.1016/j.carbon.2009.04.026

Sun, K., Ro, K., Guo, M., Novak, J., Mashayekhi, H., and Xing, B. (2011). "Sorption of bisphenol A, 17α-ethinyl estradiol and phenanthrene on thermally and hydrothermally produced biochars," *Bioresource Technol.* 102(10), 5757-5763. DOI: 10.1016/j.biortech.2011.03.038

Tu, Y., Xiong, Y., Descorme, C., Kong, L., and Tian, S. (2013). "Heterogeneous photo-Fenton oxidation of Acid Orange II over iron-sewage sludge derived carbon under visible irradiation," *J. Chem. Technol. Biot.* 89(4), 544-551. DOI: 10.1002/jctb.4151

Tu, Y., Xiong, Y., Tian, S., Kong, L., and Descorme, C. (2014). "Catalytic wet air oxidation of 2-chlorophenol over sewage sludge-derived carbon-based catalysts," *J. Hazard. Mater.* 276(9), 88-96. DOI: 10.1016/j.jhazmat.2014.05.024

Wang, H., Chen, Q. W., Yu, Y. F., Cheng, K., and Sun, Y. B. (2011). "Size-and solvent-dependent magnetically responsive optical diffraction of carbon-encapsulated superparamagnetic colloidal photonic crystals," *J. Phys. Chem. C.* 115 (23), 11427-11434. DOI: 10.1021/jp201893z

Wang, Y., Sun, H., Ang, H. M., Tadé, M. O., and Wang, S. (2014). "Magnetic Fe_3O_4/carbon sphere/cobalt composites for catalytic oxidation of phenol solutions with sulfate radicals," *Chem. Eng. J.* 245(6), 1-9. DOI: 10.1016/j.cej.2014.02.013

Xing, X., Fan, F., Shi, S., Xing, Y., Li, Y., Zhang, X., and Yang, J. (2016). "Fuel properties and combustion kinetics of hydrochar prepared by hydrothermal carbonization of corn straw," *BioResources* 11(4), 9190-9204. DOI: 10.15376/biores.11.4.9190-9204

Zhang, Z. J., Chen, X. Y., Wang, B. N., and Shi, C. W. (2008). "Hydrothermal synthesis and self-assembly of magnetite (Fe_3O_4) nanoparticles with the magnetic and electrochemical properties," *J. Cryst. Growth* 310(24), 5453-5457. DOI: 10.1016/j.jcrysgro.2008.08.064

Zhang, P., Dong, S. J., Ma, H. H., Zhang, B. X., Wang, Y. F., and Hu, X. M. (2015). "Fractionation of corn stover into cellulose, hemicellulose and lignin using a series of ionic liquids," *Ind. Crop. Prod.* 76(1), 688-696. DOI: 10.1016/j.indcrop.2015.07.037

Zhu, M., and Diao, G. (2011). "Review on the progress in synthesis and application of magnetic carbon nanocomposites," *Nanoscale* 3(7), 2748-2767. DOI: 10.1039/C1NR10165J

Zubir, N. A., Yacou, C., Motuzas, J., Zhang, X., and Costa, J. C. D. (2014). "Structural and functional investigation of grapheme oxide-Fe_3O_4 nanocomposites for the herterogeneous Fenton-like reaction," *Sci. Rep.* 4(1), 1-7. DOI: 10.1038/srep04594